IEEE Access
Multidisciplinary | Rapid Review | Open Access Journal

Received October 15, 2018, accepted November 6, 2018, date of publication November 12, 2018,
date of current version December 7, 2018.

Digital Object Identifier 10.1109/ACCESS.2018.2880569

Analysis and Improvement of Frequency Stabilization Characteristics of a Total Reflection Prism Laser Gyro

YUANBO TAO, SIHAI LI, AND SHIMING LIU
School of Automation, Northwestern Polytechnical University, Xi'an 710129, China
Corresponding author: Yuanbo Tao (taoyuanbo1990@sina.com)

This work was supported by the General Armament Department Pre-Research Fund under Grant 9140A090319.

ABSTRACT To rectify the low accuracy of frequency stabilization for a total reflection prism laser gyro (TRPLG), a mathematical model for TRPLG frequency stabilization was established. Wavelet filtering was introduced into the phase-sensitive demodulation process, with a 6-scale decomposition for the alternating current (AC) signal of light intensity used with the db4 wavelet. Combined with soft threshold and forced denoising, the signal-to-noise ratio (SNR) of the phase-sensitive signal was improved by 23.3%, with the accuracy of the frequency stabilization improved by 0.5 orders of magnitude. Increasing the variable gain in the forward channel stabilized the dynamic performance of the frequency stabilization control system. A temperature-compensated feed-forward control system was used to achieve full compensation for the temperature-induced frequency stabilization error, which also improved the accuracy of the frequency stabilization by 1 order of magnitude. Combined with wavelet filtering and feed-forward compensation, the optimized frequency stabilization control system improved the accuracy of frequency stabilization by 1.5 orders of magnitude compared with the original frequency stabilization control system in the full temperature range, and it improved the gyro's accuracy by more than 40%.

INDEX TERMS Total reflection prism laser gyro, accuracy of frequency stabilization, wavelet filtering, feed-forward control, full compensation, gyro's accuracy.

I. INTRODUCTION

An inertial navigation system is an autonomous navigation system that does not rely on any external information and does not release energy. It supports good concealment and can work in various complex environments such as the air, ground, and underwater. Laser strap-down inertial navigation systems use laser gyros as their core device and are widely used due to their high precision [1].

Three major errors exist in conventional two-mode active laser gyros: zero bias, mode locking, and scale factor error. Zero bias occurs when the frequency difference is nonzero for a zero input rate. It can be effectively reduced by temperature compensation [2], [3]. Mode locking is caused by a weak coupling mechanism between two otherwise independent traveling waves, which causes backscattering from one wave into the other, mostly at the mirrors due to surface imperfections. Compensation technology has been studied to rectify this error [4]–[7]. Scale factor error refers to variations in the scale factor as a function of the rotation rate [8]. A total reflection prism laser gyro (TRPLG) is a high-precision angular rate sensor with a total reflection prism laser as the core device [9]. It is completely free from coating, and it has the advantages of a small lock area, high reliability, long service life, etc. It has a wide range of applications in the aerospace field [10]. Studies show that the errors in a laser gyro are closely related to the resonant frequency of the laser, with the stability of the resonant frequency being a key factor affecting the performance of the laser gyro [11]–[15]. Therefore, it is important to study the frequency stabilization characteristics of TRPLGs.

The method of stabilizing the operating frequency of the laser has matured [16], mainly used in traditional laser gyros with reflectors [17]. To date, few studies have been conducted on this topic. Liu *et al.* [18] used the finite element analysis method to simulate and obtain the variation law for the temperature gradient field distribution of the resonant cavity with the mode-shifting parameters during frequency stabilization, and they optimized the control parameters. Since the TRPLG

phase-sensitive signal is susceptible to interference and a blind zone is encountered during frequency stabilization, Ma *et al.* [19], [20] applied adaptive and dual longitudinal mode frequency stabilization technologies to improve the accuracy of the frequency stabilization. From the perspective of the control system, they also proposed a type 2 third-order control system instead of the original type 1 second-order control system, thus eliminating the steady-state error under temperature ramp disturbances [21]. However, high-order systems have large overshoots, long adjustment times, and general dynamic performance. Moreover, in the case of variable temperature, the internal temperature characteristics of the gyro are not ramp signals, and they may include acceleration or even higher-order signals, thus resulting in the generation of steady-state error and reducing the accuracy of both frequency stabilization and the gyro.

During the mass production of TRPLGs, the accuracy of the frequency stabilization and the gyro's performance are often poor under variable temperatures [22]. To solve this problem, we analyzed the frequency stabilization principle of a TRPLG to establish a mathematical model for the same. Wavelet filtering was added between the TRPLG AC signal of light intensity and the finite impulse response (FIR) bandpass filter, which reduced the noise and improved the SNR of the phase-sensitive signal. Increasing the variable gain in the forward channel stabilized the dynamic performance of the system. We used a feed-forward control system to compensate the temperature-induced steady-state error to improve the steady-state performance of the system. These measures improved the accuracy of the frequency stabilization of the TRPLG, thereby providing a theoretical basis for the development and production of TRPLGs.

II. FREQUENCY STABILIZATION PRINCIPLE OF TRPLG

The frequency stabilization control system of a TRPLG is shown in Figure 1. The core component is a resonant microcrystalline glass cavity with fused silica glass prisms. The X1 channel is filled with helium neon gas mixed in a certain proportion with a working wavelength of 0.6328 μm. The laser is generated under the action of an ignition transformer and high-frequency oscillator. X2 and X4 are vacuum channels, and the X3 channel is filled with dry air. The refractive index of the air is changed by connecting the heater to stabilize the resonant frequency of the cavity. The parts marked as I, II, III and IV in the figure are prisms, which are sealed by a protective cover to keep their surfaces clean. Total reflection occurs at the prism's large inclined plane, thus ensuring minimum beam loss.

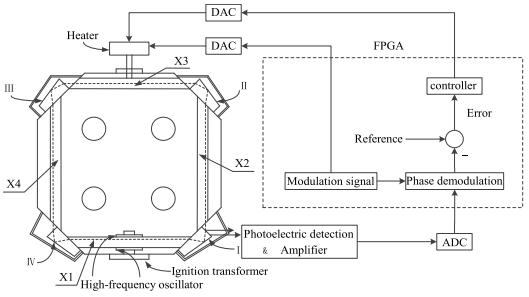

FIGURE 1. Schematic diagram of the frequency stabilization control system of a TRPLG.

Fluctuations in temperature, mechanical vibrations, and the influence of a magnetic field, etc. may cause adverse effects on the geometric length of the resonant cavity and the refractive index of the working medium. The resonant frequency of the laser is mainly determined by the resonant frequency of the resonator without considering slight variations in the atomic transition spectrum, which is defined as $\upsilon = qc/\langle L\rangle$, where q is the longitudinal mode number, c is the vacuum light speed and $\langle L\rangle$ is the optical path length of the TRPLG. The frequency of the longitudinal mode is difficult to obtain directly in the resonator. Usually, the frequency is stabilized according to the light intensity tuning curve, whose slope directly affects the accuracy of the frequency stabilization.

The relationship between the light intensity, light intensity rate and frequency parameters are shown in Figure 2 [14].

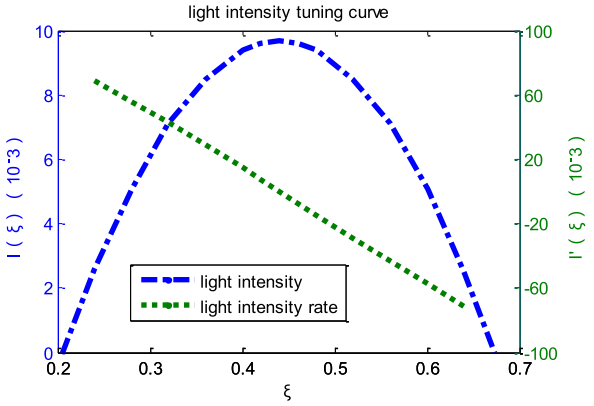

FIGURE 2. Light intensity tuning curve of TRPLG.

Based on the characteristics of the light intensity tuning curve, a sinusoidal modulated signal with a frequency of 266.7 Hz is generated by an FPGA. The piezoelectric ceramic diaphragm inside the heater is influenced by a DAC to slightly alter the resonant frequency and the frequency parameter ξ of the laser, resulting in changes in the light intensity. The accurate position of ξ can be known based on the positive and negative rate of changes in light intensity. The ultimate goal is to make ξ equal to 0.44 to achieve maximum light intensity. After the optical output beat signal is photoelectrically detected and amplified, phase-sensitive demodulation is performed after the ADC, with the phase-sensitive signal compared with the reference value to obtain the error signal, which is used as the input for the controller. The latter uses an appropriate method to generate the output signal. After the DAC, the controller acts on both ends of the heating wire inside the heater and adjusts the refractive index of the air in the X3 channel to change the length of the optical path and stabilize the frequency.

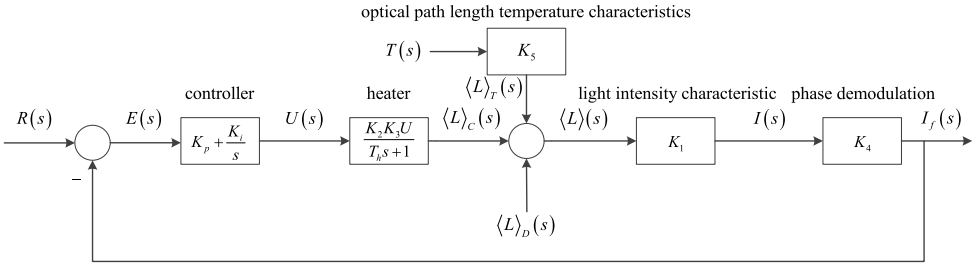

FIGURE 3. Structure diagram of a frequency stabilization control system of a TRPLG.

III. MATHEMATICAL MODEL OF THE FREQUENCY STABILIZATION SYSTEM

Under the action of a sinusoidal modulated signal, to obtain the transfer function of the changes in light intensity and the optical path length of the resonant cavity, the self-saturation effect and the mutual-saturation effect are ignored. Details of the transfer function are derived in APPENDIX A; the expression of the transfer function is $\Delta I(s)/\Delta\langle L\rangle(s) = K_1$. The transfer function between the changes in the optical path length of the X3 channel and the heater voltage is $\Delta\langle L\rangle(s)/\Delta U(s) = K_2K_3U/(T_hs+1)$; see APPENDIX B for specific parameters. The bandpass filter is used for phase-sensitive demodulation. Its transfer function is $K_4e^{-\tau s}$, with a time constant much smaller than T_h, which can be ignored. The controller uses a proportional integral algorithm with the transfer function of $\Delta U(s)/\Delta E(s) = K_p + K_i/s$. Changes in the optical path length due to temperature are given by $K_5T(s)$, and changes in the optical path length caused by a sinusoidal modulated signal are given by $\langle L\rangle_D(s)$. The structure of the frequency stabilization control system of the TRPLG is shown in Figure 3.

The open-loop transfer function of the system is defined as:

$$G(s) = \frac{K\left(\frac{K_p}{K_i}s+1\right)}{s(T_hs+1)} \tag{1}$$

where the open-loop gain $K = K_iK_1K_2K_3K_4U$.

The closed-loop transfer function of the system under the input of the control is defined as:

$$\Phi(s) = \frac{I_f(s)}{R(s)} = \frac{\frac{K}{T_h}\left(\frac{K_p}{K_i}s+1\right)}{s^2+\frac{KK_p+K_i}{K_iT_h}s+\frac{K}{T_h}} \tag{2}$$

The transfer function of the system error under the input of the control is defined as:

$$\Phi_e(s) = \frac{E(s)}{R(s)} = \frac{s\left(s+\frac{1}{T_h}\right)}{s^2+\frac{KK_p+K_i}{K_iT_h}s+\frac{K}{T_h}} \tag{3}$$

The transfer function of the system error under the input of the temperature is defined as:

$$\Phi_{eT}(s) = \frac{E(s)}{T(s)} = \frac{-\frac{K_5K_1K_4}{T_h}s(T_hs+1)}{s^2+\frac{KK_p+K_i}{K_iT_h}s+\frac{K}{T_h}} \tag{4}$$

The total system error is defined as:

$$E(s) = \Phi_e(s)R(s) + \Phi_{eT}(s)T(s) \tag{5}$$

The above equations were used to establish a mathematical model of the system. Further analysis and improvement of the performance of the system can be carried out on the basis of this model.

IV. ANALYSIS AND IMPROVEMENT OF FREQUENCY STABILIZATION CHARACTERISTICS

A. DEMODULATION OF THE PHASE-SENSITIVE SIGNAL

The demodulation of the phase-sensitive signal is crucial in the TRPLG frequency stabilization process. The SNR of the phase-sensitive signal affects the accuracy of the frequency stabilization. In addition, the phase-sensitive signal needs to be extracted from the TRPLG AC signal of light intensity, which makes the method of demodulation particularly important.

We used a TRPLG type 70 produced by Xi'an North Jierui Optoelectronics Technology Ltd. as the experimental model. The FPGA acquired the TRPLG AC signal of the light intensity at a frequency of 1 KHz in approximately 130 seconds. The converted analog data for the AC light intensity and its frequency spectrum are shown in Figure 4.

The frequency spectrum clearly showed that the TRPLG AC signal of light intensity contains a phase-sensitive signal of 266.7 Hz, a mechanical dither signal of 366 Hz, and other noise signals. To extract the phase-sensitive signal effectively, the traditional digital bandpass filtering method was adopted. The magnitude of the response of the FIR bandpass filter is shown in Figure 5.

The signal after FIR bandpass filter processing together with its frequency spectrum are shown in Figure 6. The original phase-sensitive signal contained a certain degree of noise (Figure 6b). Therefore, the elimination of noise helps to improve the accuracy of the frequency stabilization.

The optimized phase-sensitive demodulation added a wavelet filtering between the TRPLG AC signal of the light intensity and the FIR bandpass filter. Wavelet filtering was used for denoising to improve the SNR of the phase-sensitive signal. The specific design of the wavelet filter used in our study is described below.

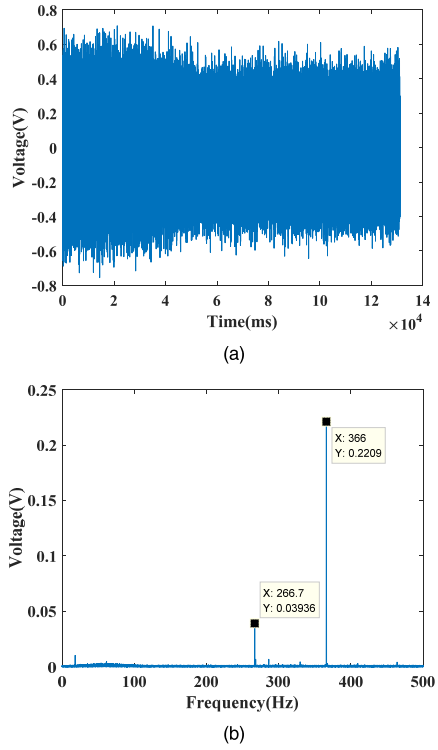

FIGURE 4. TRPLG AC signal of light intensity and its frequency spectrum: (a) AC signal of light intensity; (b) Frequency spectrum of AC signal of light intensity.

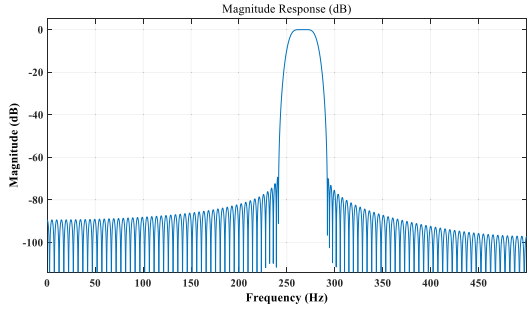

FIGURE 5. Magnitude response of the FIR bandpass filter.

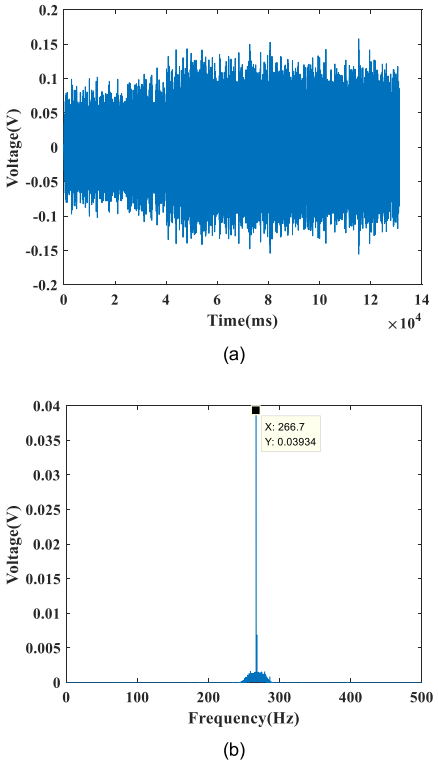

FIGURE 6. Original phase-sensitive signal and its frequency spectrum: (a) Original phase-sensitive signal; (b) Frequency spectrum of the original phase-sensitive signal.

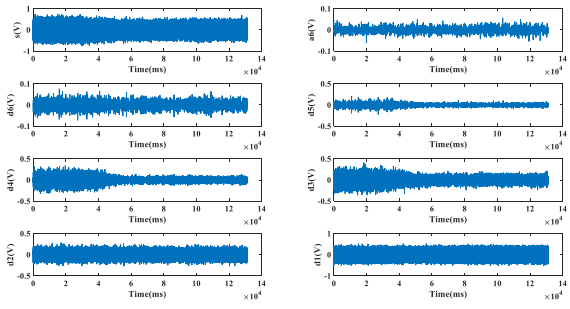

FIGURE 7. Decomposition of the TRPLG AC signal of light intensity.

For the selection of wavelet functions, a db4 wavelet with orthogonal properties was selected to ensure the effective decoupling of the wavelet coefficients in each frequency band, with 6 layers of wavelet decomposition used. The decomposition of the TRPLG AC signal of light intensity is shown in Figure 7, with the AC signal of light intensity $s = a6 + d6 + d5 + d4 + d3 + d2 + d1$; d1 and d2 were used as soft thresholds ($t = 4\sigma$) to denoising, with the other segments forced to denoise. The reconstructed signal is shown in Figure 8(a), and its spectrum is shown in Figure 8(b).

The wavelet-filtered signal after FIR bandpass filtering is shown in Figure 8(c), with its frequency spectrum shown in Figure 8(d).

To compare the optimized and original phase-sensitive demodulation, the AC signal of light intensity, and the original and optimized phase-sensitive signal were plotted, as shown in Figure 9(a). Their frequency spectra are shown in Figure 9(b). Compared to the original, the optimized phase-sensitive demodulation effectively reduced noise interference. Figure 9(c) compares their power spectral densities (PSDs), using the following expression for the SNR $10 * \mathrm{Log}_{10}$ (Signal power/Noise power), i.e., the difference between the PSD of the signal and the PSD of noise. Since the noise was mainly concentrated near the frequency of the signal, the SNR at that location was mainly analyzed. We determined the original SNR to be 29.88 dB and the optimized SNR to be 36.84 dB, with the SNR improved by 23.3%, which helps to improve the accuracy of the frequency stabilization.

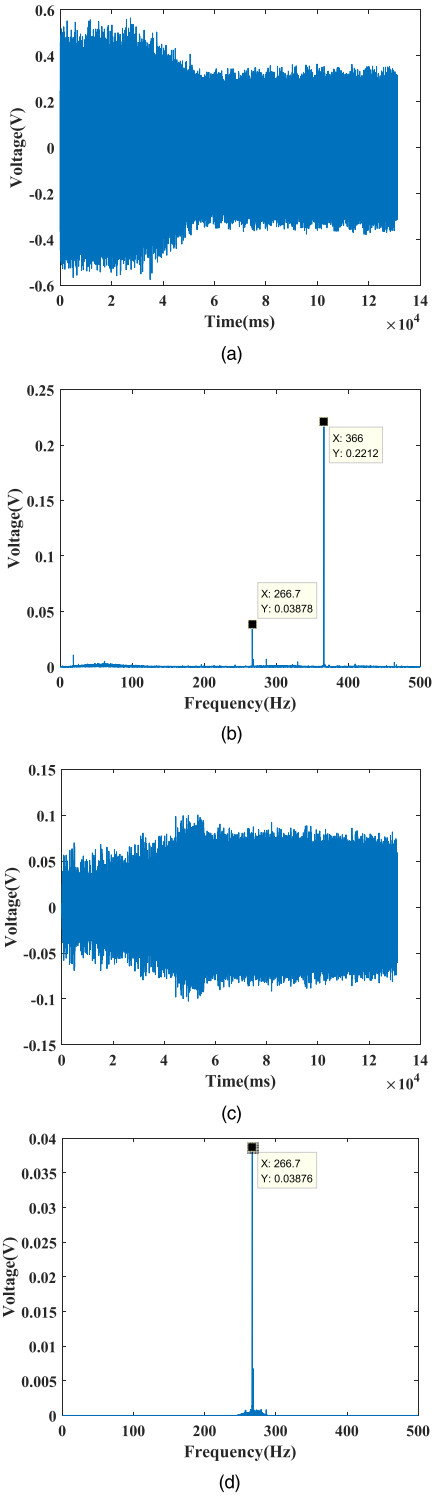

FIGURE 8. Optimized signal and its frequency spectrum: (a) Wavelet-filtered signal; (b) Frequency spectrum of the wavelet-filtered signal; (c) Optimized phase-sensitive signal; (d) Frequency spectrum of the optimized phase-sensitive signal.

B. ANALYSIS AND OPTIMIZATION OF PERFORMANCE

After the gyro was started at room temperature, the internal temperature field was steady and U was equal to 2V; then, we obtained $T_h = 0.5$ and $K = 12.250$. In the original system,

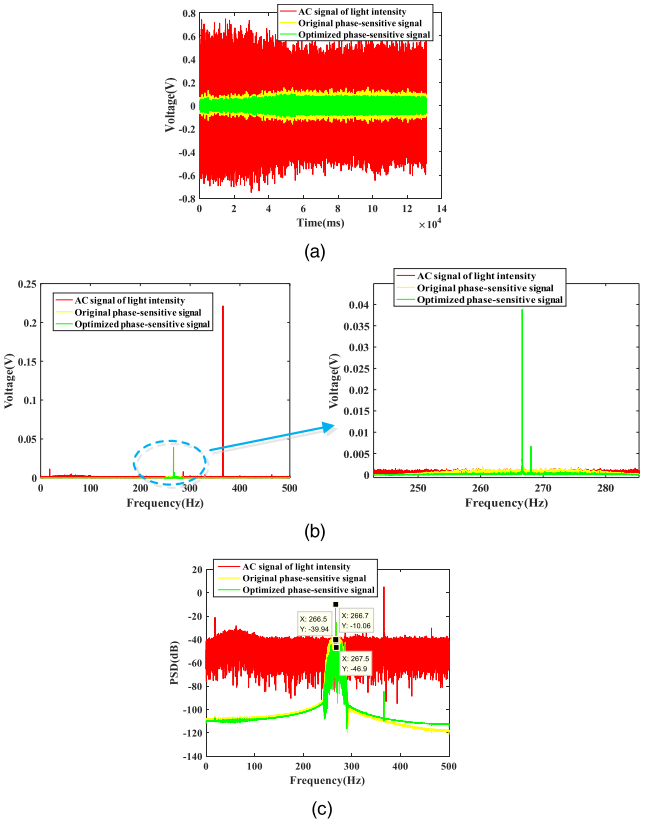

FIGURE 9. Comparison between optimized phase-sensitive demodulation and original phase-sensitive demodulation: (a) Comparison of signals; (b) Comparison of frequency spectra; (c) Comparison of PSDs.

$K_p = 4.596$ and $K_i = 22.525$; therefore,

$$G(s) = \frac{12.25\,(0.204s+1)}{s\,(0.5s+1)} \tag{6}$$

$$\Phi(s) = \frac{I_f(s)}{R(s)} = \frac{24.5\,(0.204s+1)}{s^2+7s+24.5} \tag{7}$$

Since the coefficients of the denominator in $\Phi(s)$ are all greater than 0 for this second-order system, the system must be stable according to the Rolls stability criterion.

Under typical external action, a stable system will enter a steady state after a certain period. The steady-state error of the control system is a measure of the control accuracy of the system. According to the stability theory of the linear system, the steady-state error of a type I system is 0 at the step input $r(t) = A \times 1(t)$, the steady-state error is $-AK_5/(K_iK_2K_3U)$ at the input of the temperature ramp $T(t) = At$, and the steady-state error is ∞ at the input of temperature acceleration $T(t) = At^2/2$. The TRPLG shows self-heating characteristics after starting, with the temperature field at a constant temperature approximating the input of the ramp, and the temperature field at the slow variable temperature approximately composed of the acceleration input and the ramp input segmentally. According to the principle of linear superposition, the steady-state error at the constant temperature is $e_{ssc}(\infty) = -AK_5/(K_iK_2K_3U)$, and the steady-state error at the slow variable temperature is

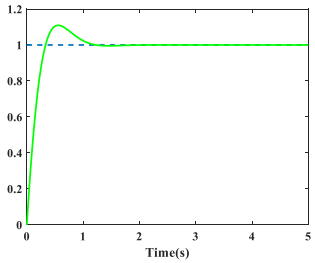

FIGURE 10. Unit step response curve of the frequency stabilization system.

$e_{ssv}(\infty) = -AK_5/(K_iK_2K_3U) + C$, where C is the cumulative error caused by the acceleration input over a period of time.

The steady-state error at a constant temperature is proportional to the rate of temperature A and inversely proportional to the heater voltage U. During the TRPLG frequency stabilization process, the longitudinal mode jumps more frequently; therefore, the heater voltage jumps more frequently. Therefore, the steady-state error will vary periodically from a small to large value. The steady-state error at variable temperature will become greater due to the introduction of the cumulative error C and the increase of the rate of temperature. Therefore, the accuracy of the TRPLG at a variable temperature is inferior to the accuracy at a constant temperature.

The quality of a control system includes its dynamic performance in addition to its steady-state performance. From formula (7), the damping ratio of this second-order system $\xi = 0.707$ and the natural frequency $\omega_n = 4.950$, with the unit step response shown in Figure 10. The values of peak time $t_p = 0.558$s, adjustment time $t_s = 0.870$s, and overshoot $\sigma\% = 11.03\%$ indicate good dynamic performance; however, the open-loop gain is variable, which affects the performance of the system.

In addition, the system has different degrees of steady-state error under constant or slow variable temperatures, which lead to the lower accuracy of frequency stabilization. Therefore, from the perspective of frequency stabilization, to further improve the accuracy of the TRPLG, it is necessary to improve the system performance and improve the accuracy of the frequency stabilization.

To maintain the dynamic performance, as shown in Figure 10, a proportional link $K^* = 2/U$ was added into the system's forward channel to keep the system's open-loop gain constant.

To completely eliminate the system error caused by temperature and improve the accuracy of the frequency stabilization, a feed-forward control system based on temperature compensation was used to introduce the temperature into a closed loop through the feed-forward channel. The transfer function of the feed-forward channel $G_T(s)$ was designed so that the system output was not affected by disturbances. The system structure diagram is shown in Figure 11.

Under a temperature disturbance, the system error is as follows:

$$E(s) = -\frac{K_5K_1K^*K_4 + G_T(s)\left(K_p + \frac{K_i}{s}\right)\frac{K_2K_3U}{T_hs+1}K_1K^*K_4}{1 + \frac{K\left(\frac{K_p}{K_i}s+1\right)}{s(T_hs+1)}}T(s) \tag{8}$$

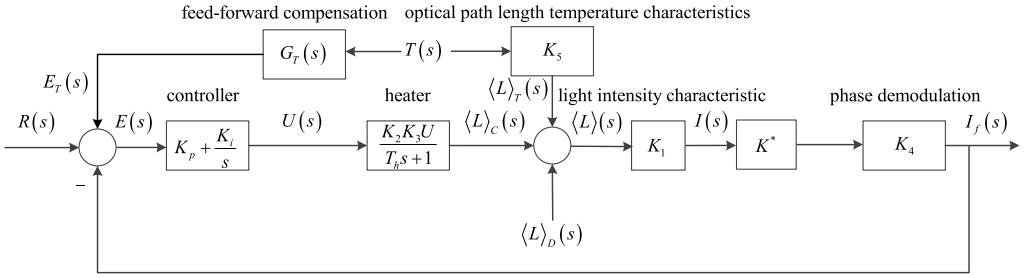

FIGURE 11. Structure diagram of a feed-forward control system based on temperature compensation.

TABLE 1. Comparison between the original control system and the system with wavelet filtering.

Temperature (℃)	Original control system		System with wavelet filtering		Improvement	
	Gyro's accuracy (°/h)	Accuracy of frequency stabilization	Gyro's accuracy (°/h)	Accuracy of frequency stabilization	Gyro's accuracy percentage	Accuracy of frequency stabilization
-40	0.0107	1.8×10^{-7}	0.0091	5.1×10^{-8}	15.0%	$1.11\times10^{0.5}$
25	0.0092	1.4×10^{-7}	0.0079	4.1×10^{-8}	14.1%	$1.08\times10^{0.5}$
70	0.0096	1.6×10^{-7}	0.0082	5.0×10^{-8}	14.6%	$1.01\times10^{0.5}$
-40～70	0.0142	2.3×10^{-7}	0.0120	6.4×10^{-8}	15.5%	$1.14\times10^{0.5}$
70～-40	0.0150	2.4×10^{-7}	0.0127	6.6×10^{-8}	15.3%	$1.15\times10^{0.5}$

TABLE 2. Comparison between the original control system and the system with feed-forward compensation.

Temperature (℃)	Original control system		System with feed-forward compensation		Improvement	
	Gyro's accuracy (°/h)	Accuracy of frequency stabilization	Gyro's accuracy (°/h)	Accuracy of frequency stabilization	Gyro's accuracy percentage	Accuracy of frequency stabilization
-40	0.0107	1.8×10^{-7}	0.0073	1.6×10^{-8}	31.8%	1.13×10^{1}
25	0.0092	1.4×10^{-7}	0.0062	1.3×10^{-8}	32.6%	1.08×10^{1}
70	0.0096	1.6×10^{-7}	0.0067	1.4×10^{-8}	30.2%	1.14×10^{1}
-40～70	0.0142	2.3×10^{-7}	0.0095	2.0×10^{-8}	33.1%	1.15×10^{1}
70～-40	0.0150	2.4×10^{-7}	0.0101	2.1×10^{-8}	32.7%	1.14×10^{1}

TABLE 3. Comparison between the original control system and the optimized control system.

Temperature (℃)	Original control system		Optimized control system		Improvement	
	Gyro's accuracy (°/h)	Accuracy of frequency stabilization	Gyro's accuracy (°/h)	Accuracy of frequency stabilization	Gyro's accuracy percentage	Accuracy of frequency stabilization
-40	0.0107	1.8×10^{-7}	0.0063	5.6×10^{-9}	41.1%	$1.02\times10^{1.5}$
25	0.0092	1.4×10^{-7}	0.0053	4.3×10^{-9}	42.4%	$1.03\times10^{1.5}$
70	0.0096	1.6×10^{-7}	0.0057	4.9×10^{-9}	40.6%	$1.03\times10^{1.5}$
-40～70	0.0142	2.3×10^{-7}	0.0082	7.2×10^{-9}	42.3%	$1.01\times10^{1.5}$
70～-40	0.0150	2.4×10^{-7}	0.0086	7.5×10^{-9}	42.7%	$1.02\times10^{1.5}$

If $G_T(s) = -K_5(T_h s+1)/\left[K_2K_3U\left(K_p+K_i/s\right)\right]$, the $E(s) = 0$, indicating full compensation for the error caused by temperature, elimination of the steady-state error at constant temperature and slow variable temperature, and improvement in the accuracy of the frequency stabilization of the overall response process.

For temperature compensation in the device, a PT100 was used to convert the temperature into a resistance, which became the voltage signal through a signal-conditioning circuit. Therefore, the FPGA controls the ADC to acquire it. The signal-conditioning circuit consisted of a bridge circuit, an operational amplifier, and a low-pass filter, as shown in Figure 12. The linear expression of the corrected temperature is $T = 0.00294 \times \text{AD\_VALUE} + 38.2$, where the AD_VALUE is a 16-bit signed number obtained by the analog-to-digital conversion.

After starting the gyro at room temperature, it was tested for 0.5h under the premise of no feed-forward compensation, with the temperature $T(t)$, heater voltage $U(t)$ and system error $e_{ss}(t)$ all measured in real time. According to the control theory, the system error under the action of a temperature disturbance is given as follows:

$$e_{ss}(t) = -[K_5 dT(t)/dt]/[K_i K_2 K_3 U(t)] \tag{9}$$

Substituting $T(t)$, $U(t)$, $e_{ss}(t)$ and K_i gives $K_5/(K_2K_3) \approx 0.5631$. Therefore, the transfer function of the feed-forward channel is

$$G_T(s) = \frac{E_T(s)}{T(s)} = -\frac{0.5631s(0.5s+1)}{U(4.596s+22.525)} \tag{10}$$

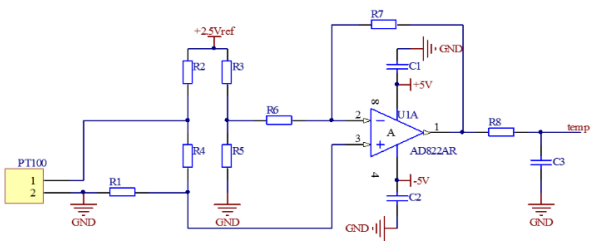

FIGURE 12. Signal-conditioning circuit of temperature.

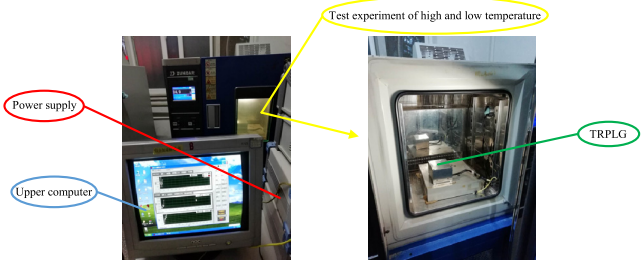

FIGURE 13. Experimental platform of the TRPLG.

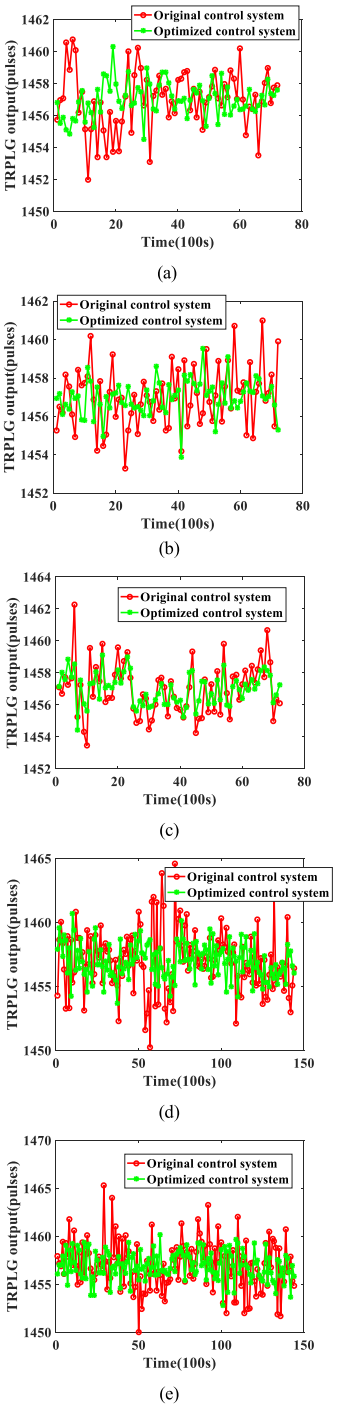

FIGURE 14. TRPLG output at different temperatures: (a) at −40 °C; (b) at +25 °C; (c) at +70 °C; (d) at −40 ∼ +70 °C; (e) at +70 ∼ −40 °C.

C. ANALYSIS OF EXPERIMENTAL RESULTS

To further verify the theoretical analysis and simulation, the original frequency stabilization control system, the system with wavelet filtering and the system with feed-forward compensation were used to test the performance of the TRPLG at high and low temperatures. It was tested for 2 h at constant temperature and for 4 h at variable temperature at a rate of 1 °C/min. The accuracy of the frequency stabilization was based on using an iodine-stabilized laser as the frequency standard, using the beat frequency principle for detection. The experimental platform is shown in Figure 13, with the test results shown in Table 1 and Table 2.

The experimental results showed that the system with wavelet filtering can improve the accuracy of the frequency stabilization by 0.5 orders of magnitude compared to the original frequency stabilization control system, with the gyro's accuracy improved by more than 14% (Table 1). In addition, the system with feed-forward compensation can be used to improve the accuracy of the frequency stabilization by 1 order of magnitude compared to the original frequency stabilization control system, with the gyro's accuracy improved by more than 30% (Table 2). It can be clearly seen that the feed-forward compensation was better than the wavelet filtering in improving the accuracy of the frequency stabilization.

Based on the above results, the original frequency stabilization control system was optimized by the combination of wavelet filtering and feed-forward compensation. The TRPLG output is shown in Figure 14, with the optimized results shown in Table 3.

Compared to the original, the optimized frequency stabilization control system decreased the fluctuations in the TRPLG output and increased the stability in the full temperature range.

The results showed that the optimized frequency stabilization control system could be used to improve the accuracy of the frequency stabilization by 1.5 orders of magnitude compared to the original frequency stabilization control system, with the gyro's accuracy improved by more than 40% (Table 3). Therefore, the combination of wavelet filtering and feed-forward compensation is optimal.

V. CONCLUSIONS

We analyzed the working principle for a TRPLG frequency stabilization control system and established a mathematical model of the same. According to the open-loop transfer function for the system, it is a type 1 second-order control system. An FIR bandpass filter was used as the demodulation filter for the system phase-sensitive signal. After processing and analyzing the TRPLG AC signal of light intensity, the phase-sensitive signal was greatly disturbed by noise. By analyzing the dynamic and steady-state performance of the system, we found that the open-loop gain of the system varied with the heater voltage and affected the dynamic performance. The steady-state error at constant temperature was proportional to the rate of temperature and inversely proportional to the heater voltage. The steady-state error at variable temperature increased due to the introduction of the cumulative error and increase in the rate of temperature.

To address the shortcomings of the original frequency stabilization system, we introduced wavelet filtering in the demodulation of the phase-sensitive signal, which effectively reduced the noise in the pass-band and improved the SNR of the phase-sensitive signal. Increasing the variable gain in the forward channel stabilized the dynamic performance of

the frequency stabilization control system. A temperature-compensated feed-forward control system achieved full compensation for the temperature-induced steady-state error. The optimized frequency stabilization control system improved the accuracy of the frequency stabilization by 1.5 orders of magnitude compared to the original system in the full temperature range and improved the gyro's accuracy by more than 40%.

APPENDIX

A. RELATIONSHIP BETWEEN LIGHT INTENSITY AND OPTICAL PATH LENGTH

Under the condition of Doppler-based broadening, gyro light intensity is calculated as follows:

$$I(\xi) = I_m e^{-\xi^2} \tag{11}$$

where I_m is the maximum gain of light intensity and $\xi = (\omega - \omega_0)/(ku)$.

Differentiating (11), we have

$$\frac{dI}{d\omega} = \frac{dI}{d\xi}\frac{d\xi}{d\omega} = -2I\frac{\omega - \omega_0}{(ku)^2} \tag{12}$$

Since $d\omega/d\langle L\rangle = -\omega/\langle L\rangle$,

$$\Delta I(s)/\Delta\langle L\rangle(s) = K_1 \tag{13}$$

where $K_1 = 2I\frac{\omega-\omega_0}{(ku)^2}\frac{\omega}{\langle L\rangle}$.

B. CHARACTERISTICS OF THE HEATER

The heater structure is illustrated in Figure 15.

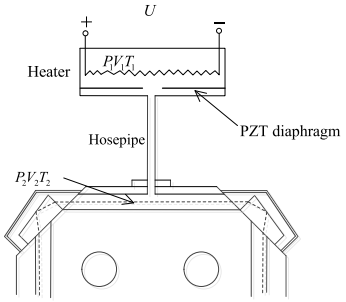

FIGURE 15. Structure diagram of the heater.

To obtain the transfer function for the changes in the optical path length of the X3 channel and the heater voltage, the law of thermodynamics is applied as follows:

$$CM\frac{d(\Delta T)}{dt} + HA\Delta T = \Delta Q \tag{14}$$

where the quality of the heater is M, the specific heat is C, the coefficient of heat transfer is H, the area of heat transfer is A, the air temperature inside the heater is T, the voltage across the heating wire is U, the resistance of the heating wire is R, and the heat generated by the heating wire per unit time is Q.

Since $Q = U^2/R$, there is a nonlinear relationship between Q and U, which can be linearized near the balance point (Q_0, U_0), which is calculated as $\Delta Q = 2U\Delta U/R$, so

$$\frac{CM}{HA}\frac{d(\Delta T)}{dt} + \Delta T = \frac{2U}{RHA}\Delta U \tag{15}$$

If the time constant of the heater is $T_h = CM/(HA)$, then

$$\frac{\Delta T(s)}{\Delta U(s)} = \frac{K_2 U}{T_h s + 1} \tag{16}$$

where $K_2 = \frac{2}{RHA}$.

According to the state equation for an ideal gas, $P_1V_1 = N_1RT_1/N_A$ and $P_2V_2 = N_2RT_2/N_A$, where P_1 is the internal pressure of the heater, V_1 is the volume of the gas, N_1 is the number of molecules, T_1 is the temperature, P_2 is the internal pressure of the X3 channel, V_2 is the volume of the gas, N_2 is the number of molecules, T_2 is the temperature, N_A is Avogadro's constant, and R is the Molar gas constant. When $P = P_1 = P_2$, then $V_1/V_2 = N_1T/(N_2T_2)$, and the relationship between the temperature changes of the heater and the changes in density of the gas molecular number in the X3 channel is described by:

$$\Delta n_2 = \frac{\Delta N_2}{V_2} = \frac{N_1}{V_1T_2}\Delta T_1 \tag{17}$$

The relationship between the air refractive index and the density of the molecular number in the X3 channel is $n_a = 1 + (\alpha n_2)/(2\varepsilon_0)$, where α is the average polarizability for air and ε_0 is the vacuum capacitance ratio. Combining this with equation (17):

$$\Delta\langle L\rangle(s)/\Delta T(s) = K_3 \tag{18}$$

where $K_3 = \frac{\alpha L_2}{2\varepsilon_0}\frac{N_1}{V_1T_2}$.

In summary, the transfer function for the change in the optical path length of the frequency stabilization channel and the heater voltage variation is

$$\frac{\Delta\langle L\rangle(s)}{\Delta U(s)} = \frac{K_2K_3U}{T_hs + 1} \tag{19}$$

REFERENCES

[1] Q. G. Jiang, W. Q. Wu, M. M. Jiang, and Y. Li, "A new filtering and smoothing algorithm for railway track surveying based on landmark and IMU/odometer," *Sensors*, vol. 17, no. 6, p. 1438, Jun. 2017.

[2] G. Li, F. Wang, G. Xiao, G. Wei, P. Zhang, and X. Long, "Temperature compensation method using readout signals of ring laser gyroscope," *Opt. Express*, vol. 23, no. 10, pp. 13320–13332, May 2015.

[3] X. Yu, Y. Wang, G. Wei, P. Zhang, and X. Long, "Novel temperature modeling and compensation method for bias of ring laser gyroscope based on least-squares support vector machine," *Chin. Opt. Lett.*, vol. 9, no. 5, p. 051201, May 2011.

[4] H. P. Yu, W. Wu, M. Wu, G. Feng, and M. Hao, "Systematic angle random walk estimation of the constant rate biased ring laser gyro," *Sensors*, vol. 13, no. 3, pp. 2750–2762, Feb. 2013.

[5] Z. Fan, H. Luo, S. Hu, and G. Xiao, "Research on lock-in correction for mechanical dithered ring laser gyro," *Opt. Eng.*, vol. 50, no. 3, p. 034403, Mar. 2011.

[6] S.-W. Song, J.-C. Lee, S.-K. Hong, and D. Chwa, "New random walk reduction algorithm in ring laser gyroscopes," *J. Opt.*, vol. 12, no. 11, p. 115501, Sep. 2010.

[7] R. B. Hurst, N. Rabeendran, K. U. Schreiber, and J.-P. R. Wells, "Correction of backscatter-induced systematic errors in ring laser gyroscopes," *Appl. Opt.*, vol. 53, no. 31, pp. 7610–7618, Oct. 2014.

[8] F. Aronowitz, J. Killpatrick, and S. Callaghan, "Power-dependent correction to the scale factor in the laser gyro," *IEEE J. Quantum Electron.*, vol. 10, no. 2, pp. 201–208, Feb. 1974.
[9] C.-K. Yao, X.-D. Zeng, and C.-Q. Cao, "Intensity properties of output light in prisms laser gyro with mechanical dither bias," *Acta Phys. Sinica*, vol. 61, no. 9, p. 094216, Sep. 2012.
[10] Y. V. Bakin, G. N. Ziouzev, and M. B. Lioudomirski, *Laser Gyros With Total Reflection Prisms*. Moscow, Russia: Moscow Bauman State Technical Univ., 2003, pp. 11–29.
[11] Y. Cheng-Kang, Z. Xiao-Dong, and C. Chang-Qing, "Polarization properties in a prism laser gyro with mechanical dither bias," *Chin. Phys. B*, vol. 21, no. 12, p. 124206, Dec. 2012.
[12] W. W. Chow, J. Gea-Banacloche, L. M. Pedrotti, V. E. Sanders, W. Schleich, and M. O. Scully, "The ring laser gyro," *Rev. Mod. Phys*, vol. 57, no. 1, pp. 61–104, Jan. 1985.
[13] L. N. Menegozzi and W. E. Lamb, Jr., "Theory of a ring laser," *Phys. Rev. A, Gen. Phys.*, vol. 8, no. 4, pp. 2103–2125, Apr. 1985.
[14] Y. N. Jiang, *Ring Laser Gyro*. Beijing, China: Tsinghua Univ. Press, 1985, pp. 214–216.
[15] A. Beghi *et al.*, "Compensation of the laser parameter fluctuations in large ring-laser gyros: A Kalman filter approach," *Appl. Opt.*, vol. 51, no. 31, pp. 7518–7528, Oct. 2012.
[16] P. H. Lee and M. L. Skolnick, "Laser frequency stabilization system and method," U.S. Patent 3 697 887 A, Oct. 10, 1972.
[17] U. K. Schreiber, C. H. Rowe, D. N. Wright, S. J. Cooper, and G. E. Stedman, "Precision stabilization of the optical frequency in a large ring laser gyroscope," *Appl. Opt.*, vol. 37, no. 36, pp. 8371–8381, Dec. 1998.
[18] J. N. Liu, J. B. Jiang, S. X. Shi, J. J. Ma, and Q. Guo, "Optimization analysis of frequency stabilization servo system of prisms laser gyro," *Acta Armamentarii*, vol. 34, no. 7, pp. 821–827, Jul. 2013.
[19] J. J. Ma, J. Jiang, and J. Liu, "Frequency stabilization technique of total reflection prism laser gyros with double longitudinal modes," *Chin. J. Lasers*, vol. 41, no. 9, p. 0902011, Sep. 2014.
[20] J. J. Ma, J. B. Jiang, and J. N. Liu, "Adaptive frequency stabilization technique for total reflection prism laser gyros," *Acta Optica Sinica*, vol. 35, no. 3, p. 0314002, Mar. 2015.
[21] J. J. Ma and J. B. Jiang, "Research on the frequency stabilization properties of total reflection prism laser gyros," *Chin. J. Lasers*, vol. 42, no. 1, p. 0102002, Jan. 2015.
[22] H. Luo, S. J. Guo, S. M. Hu, G. M. Xu, and G. Li, "Research and design on high-precision frequency-stability measurement system of ring laser gyroscope," *J. Chin. Inertial Technol.*, vol. 13, no. 6, pp. 86–89, Dec. 2005.

YUANBO TAO was born in Xi'an, Shaanxi, China, in 1990. He received the B.S. degree in automation from the Xi'an University of Architecture and Technology in 2012 and the M.S. degree in detection technology and automation from Northwestern Polytechnical University, Xi'an, in 2015, where he is currently pursuing the Ph.D. degree in instrument science. His research focuses on laser gyro digital circuits and control algorithms.

SIHAI LI was born in 1962. He received the B.S. and M.S. degrees in gyroscope and inertial navigation and the Ph.D. degree in navigation, guidance and control from Northwestern Polytechnical University, Xi'an, China, in 1983, 1988, and 2000, respectively.

From 1983 to 1985, he was an Assistant Engineer with the inertial navigation system LABS. From 1988 to 1992, he was an Engineer, and from 1992 to 1994, he was a Senior Engineer. From 1994 to 1995, he was a Visiting Scholar at the University of Calgary, Canada. From 1995 to 2000, he was a Researcher with the inertial navigation system LABS. From 2000 to 2008, he was the Chief Engineer of Chenxi Aviation Technology Co. Ltd. Since 2008, he has been a Professor at Northwestern Polytechnical University and became a Doctoral Supervisor in 2013. His research interests include inertial system alignment, navigation and calibration technology, integrated navigation and navigation system information fusion technology and application, and civil aircraft navigation system.

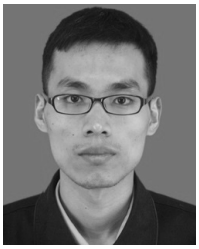

SHIMING LIU was born in Zhoukou, Henan, China, in 1988. He received the B.S. and M.S. degrees in aircraft design from Beihang University in 2010 and 2013, respectively. He is currently pursuing the Ph.D. degree in instrument science at Northwestern Polytechnical University, Xi'an, China. His research interests include alignment, integrated navigation, and information fusion.